Research Paper

Developing stretchable and graphene-oxide-based hydrogel for the removal of organic pollutants and metal ions

Chencheng Dong, Jie Lu, Bocheng Qiu, Bin Shen, Mingyang Xing*, Jinlong Zhang*

Key Laboratory for Advanced Materials and Institute of Fine Chemicals, School of Chemistry and Molecular Engineering, East China University of Science and Technology, 130 Meilong Road, Shanghai 200237, PR China

ABSTRACT

It remains challenging to process the industrial wastewater of high consistence of organic pollutants and difficult decomposition of heavy metal ions. In this study, we develop a functional nanocomposite hydrogel with a highly photocatalytic Fenton reaction activity for the degradation of organic pollutants and adsorption for the heavy metal ions. The hydrogel is made up of Fe_3O_4 nanoparticles, reduced graphene oxide (RGO) and polyacrylamide (PAM), which is prepared by a two-step chemical synthetic method, and exhibits the outstanding mechanical strength, Photo-Fenton activity, adsorptive property and reversibility. For the degradation of organic dyes, the Fe_3O_4/RGO/PAM hydrogel can degrade the 20 mg/L Rhodamine B (RhB) for 90% within 60 min under visible light irradiation, and even after 10 times cycle test, the degradation rate for RhB still keeps at 90%. Meanwhile, it can degrade the actual sewage of fine chemical wastewater, whose COD (Chemical Oxygen Demand) decreases from 10400 to 2840 mg/L after one hour's visible irradiation. For the synchronous removal of organic pollutants and heavy metal ions over hydrogel, the degradation data of 20 mg/L RhB can be up to 90% with 20 min under visible light irradiation, and the removal rate of various metal ions can reach up to 34.8%–66.3% after continual two days' adsorption. This study provides a new pathway to process the industrial wastewater of high consistence and difficult decomposition.

1. Introduction

The wastewater coming from electrolysis, electroplating, pesticide, medicine, paint, paper making, printing and dyeing, textiles and other chemical industries has done great harms to the ecological environment. That because the industrial wastewater always contains the organic pollutants and heavy metal ions, which are difficult to be degraded by the power of nature. Several traditional approaches like Fenton reaction [1,2], biological treatment [3,4], membrane technology [5], extraction [6], electrodialysis process [7] etc. have a certain effect on the treatment of organic pollutants or heavy metal ions. However, there is less report on the pollution treatment technology for the synchronous removal of organic pollutants and heavy metal ions. Polymeric hydrogels are the typical fascinating and versatile soft materials with wide potential applications in drug delivery and tissue engineering [8–11], releasing matrices for drug delivery [12], cell modulating substances [13], as well as the adsorption of heavy metals [14]. The network structure of hydrogels provides a 3D environment with high water retention, tunable mechanical properties and nutrients [15], which has a large application potential in the environment.

Unfortunately, the majority of polymeric hydrogels suffers from poor mechanical performance, which is difficult to be recycled and greatly limits its practical applications.

Recently, much attention has been paid to prepare the hydrogels with superior mechanical properties [16]. Commonly, there are three types of recipes to prepare the hydrogels, which are equipped with high strength, including a topological (TP) gel [17], a double network (DN) gel [18], and a nanocomposite (NC) gel [19]. Among of them, nanocomposite gels are considered to effectively enhance the mechanical properties of hydrogels. For instance, the nanocomposite gels with a unique organic-inorganic network structure would have the extraordinary mechanical property [20]. Nowadays, graphene oxide (GO) has been no doubt one of the hottest research topic among chemists, ascribed to its low cost for mass production and good dispersibility in water [21–24]. Meanwhile, its abundant oxygen-containing groups, *i.e.* hydroxyl, epoxide and carboxyl groups make it favorable candidates for improving the mechanical strength of the polymeric hydrogels. Ye et al. [25] have reported super tough graphene oxide (GO)-poly(acrylic acid) (PAA) nanocomposite hydrogels by using Fe^{3+} ions as cross-linkers. In regard with this, the GO-PAA nanocomposite hydrogels exhibit superior

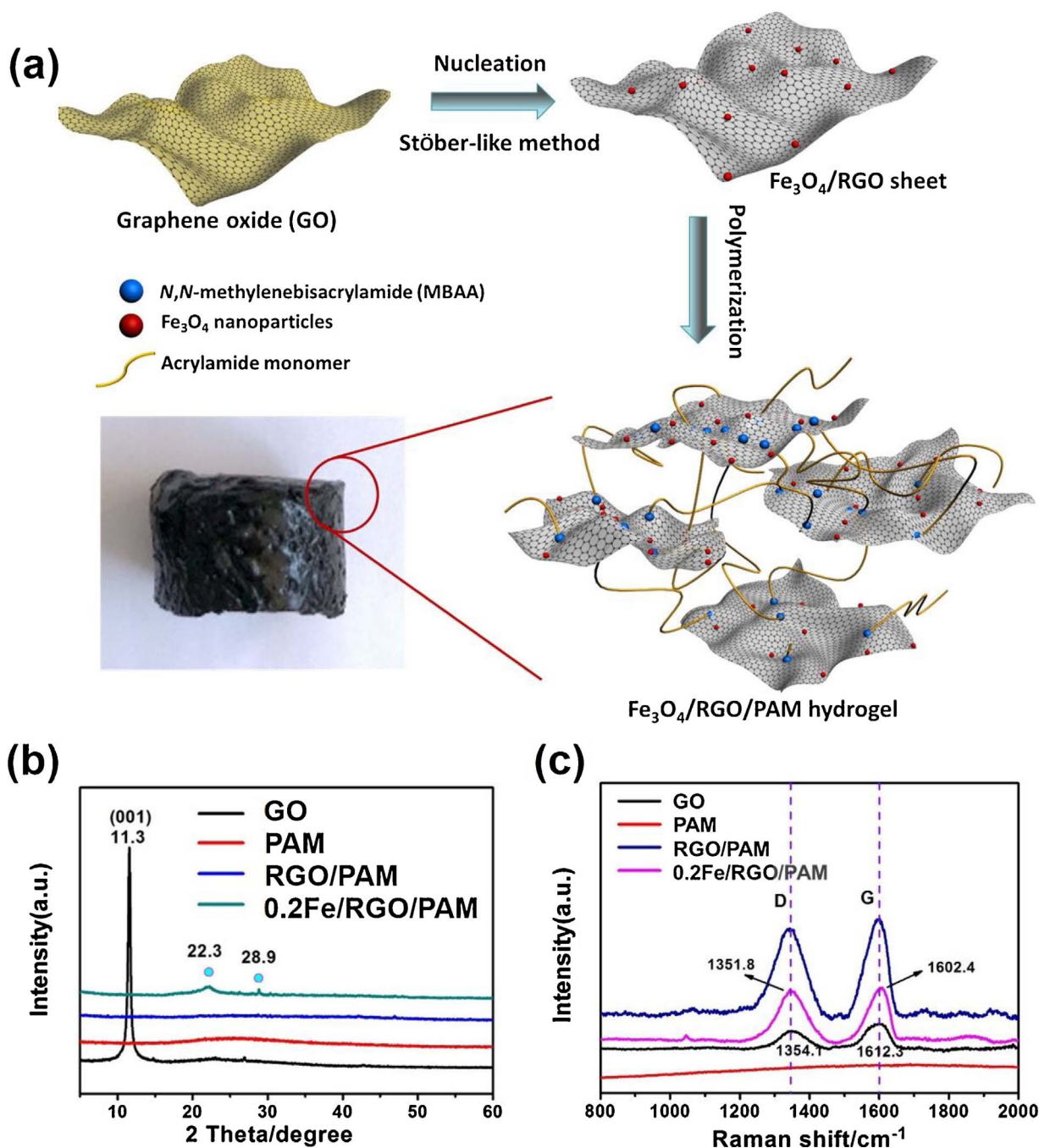**Fig. 1.** (a) Schematic steps of preparation of Fe_3O_4/RGO/PAM hydrogels, and the corresponding (b) XRD and (c) Raman spectra of hydrogels.

toughness (tensile strength = 777 kPa, work of extension = 11.9 MJ m^{-3}) and stretchability (elongation at break = 2980%). In 2012, Liu et al. [26] prepared polyacrylamide (PAM)/graphene oxide nanocomposite hydrogels (PGH) with GO nanosheets as cross-linkers, via in situ free radical polymerization of acrylamide in an aqueous suspension of GO. On the basis of that, Yu et al. [27] proposed a facile approach to prepare a new kind of elastic GO/PAM hydrogels with exceptional mechanical behavior by combination of the characteristics of conventional double-network hydrogel and nanocomposite hydrogel, thus obtaining highly elastic and super-stretchable GO/PAM hydrogels. Under this circumstance, the majority of work correlated with PAM hydrogels is to enhance its mechanical property. It is well known that GO itself has a huge surface area, good chemical stability, and graphitized basal plane structure, thus allowing it to have strong p-p interactions with the aromatic moieties present in

many organic molecule dyes [28]. Yin et al. [29] prepared graphene oxide (GO)/sodium alginate (SA)/polyacrylamide (PAM) (GO/SA/PAM) composite hydrogels, which were successfully applied in dye adsorption, including cationic dyes (R6G, MB, MG, and BG) and anionic dyes (CA, MO, BR and RB). However, the majority of the researches based on GO hydrogels focus on the adsorption of organic pollutions. PAM is a type of water-soluble polymer and widely used in industrial water treatment. And it is considered as non-toxic, economic and efficient, has undoubtedly of great potential application prospect [30]. And polyacrylamide (PAM) is composed of large numbers of amide side groups, which is beneficial for the adsorption of heavy metal ions. Although GO/Fe_3O_4 based hydrogels have been reported, Fe_3O_4/RGO/PAM hydrogel is much more efficient to adsorb heavy metals. This is because of the chemical adsorption, ascribed to the metal-NH_2 complex [31]. In the strict sense of the word, the toxicity of pollutants remains
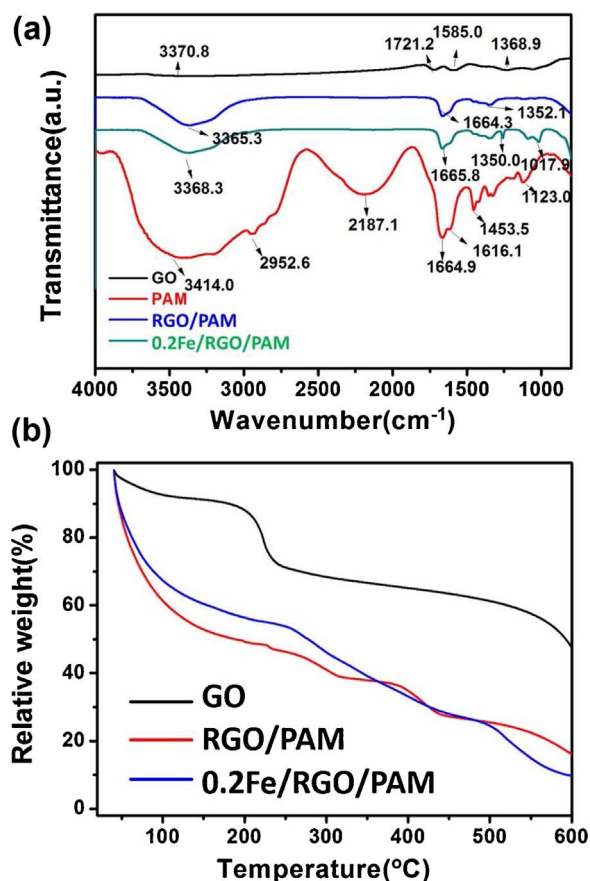
Fig. 2. (a) FTIR transmittance spectra and (b) TGA analysis of GO powders, PAM, RGO/PAM and 0.2Fe/RGO/PAM hydrogels.

Fig. 4. Compress stress (σ)- compress strain (ε) plot of PAM hydrogel and 0.2Fe/GO/PAM hydrogel.

unsolved, owing to that the organic molecules adsorbed on the hydrogels have not been really degraded. There is thereby an urgent need but it is still a significant challenge to rationally design and delicately tailor the functional hydrogels with degradation of organic pollutants
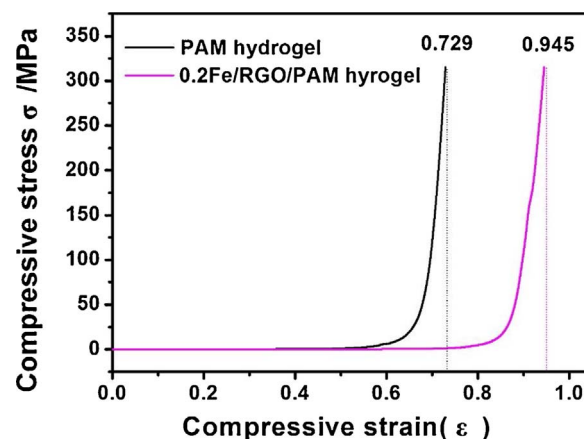
and adsorption of heavy metal ions.

In this work, we proposed a two-step method to synthesize a functional nanocomposite hydrogel with a highly photocatalytic Fenton reaction activity. It means that we employed a facile Stöber-like method to prepare the highly-dispersed Fe_3O_4 nanoparticles on the reduced graphene oxide (RGO) sheets, which were then compounded with the polyacrylamide (PAM) to obtain a polymeric hydrogel of Fe_3O_4/RGO/ PAM, by using N, N-methylenebisacrylamide (MBAA) and ammonium persulfate as the crosslinker and initiator, respectively. The obtained hydrogel has the superior stretchability, high Photo-Fenton-reaction for the degradation of organic pollutants (RhB and benzenoid wastewater), good adsorption for the heavy metal ions (Ce^{3+}, Cu^{2+}, $Ag+$, Cd^{2+}), and recyclable performance. The Fe_3O_4/RGO/PAM can synchronously remove the RhB and heavy metal ions under the visible light irradiation. The degradation data of RhB still keeps up to 90% even after 10th cyclic test, and the removal rate of various metal ions could reach to 34.8%~66.3% after two days of adsorption. Furthermore, the hydrogel also can deal with the fine chemical wastewater, whose COD was decreased from 10400 mg/L to 2840 mg/L after one hour's visible
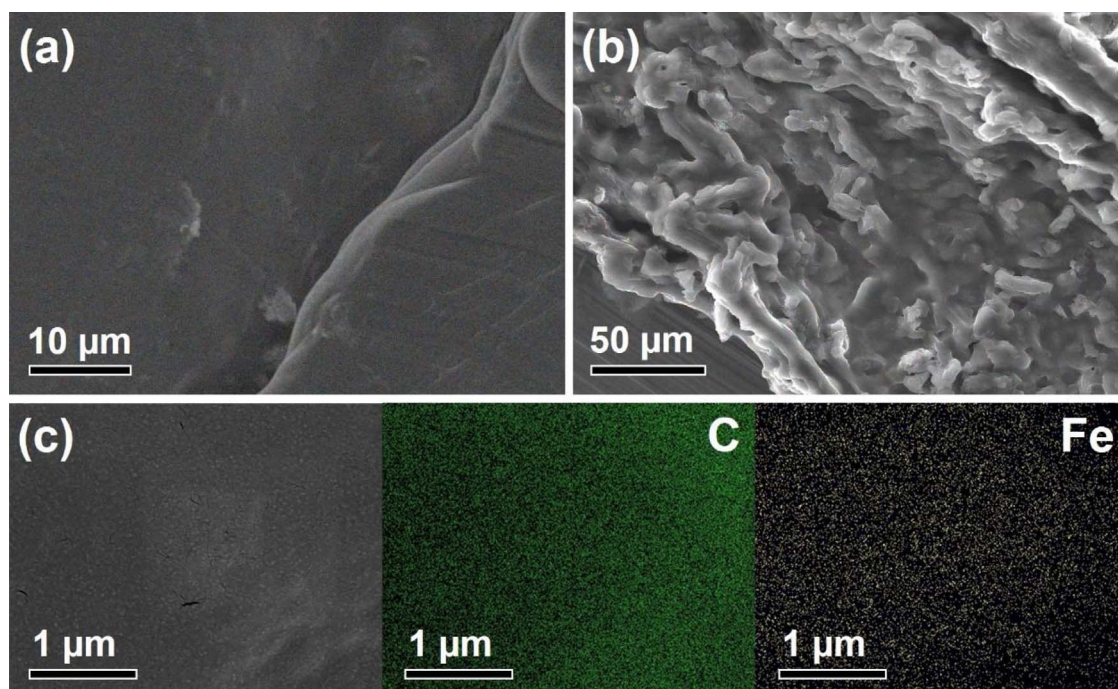

Fig. 3. SEM images for (a) RGO/PAM and 0.2Fe/RGO/PAM hydrogels, and (c) the corresponding EDS-mapping images of 0.2Fe/RGO/PAM hydrogel.

irradiation.

2. Materials and methods

2.1. Chemical reagents

All chemicals, including $NaNO_3$ (AR), H_2SO_4 (AR), $KMnO_4$ (AR), H_2O_2 (AR), HCl (AR), concentrated ammonia solution (~28 wt%), acetylacetonate $Fe(acac)_3$, acetonitrile (AR), ethanol (AR) were used as received without any further purification. Graphite powders (74 μm) were purchased from Qingdao Jinrilai Graphite Co., Ltd., $Ca(NO_3)_2$ (AR), acrylamide (AM) monomer, N,N-methylenebisacrylamide (MBAA) and ammonium persulfate, N_2, deionized water, rhodamine B (RhB), industrial wastewater, Hach reagent.

2.2. Preparation of Fe_3O_4/RGO nanocomposites

A GO dispersion was firstly prepared by using a modified Hummers' method [32,33]. The highly dispersed Fe_3O_4/RGO nanocomposites were prepared via our previous work [24]. 100 mL GO-ethanol solution was mixed with 25 mL acetonitrile in an ultrasound bath for 90 min, and then 0.1 mL of $NH_3·H_2O$ was added into the suspension at room temperature. After stirring for 30 min, 10 mL $Fe(acac)_3$/ethanol (0.2 mol L^{-1}) was added slowly into the above solution and then continue stirring for another 30 min. The suspension was maintained at 60 °C for 12 h to form the amorphous Fe_3O_4 nanoparticles pre-growth on the RGO sheets.

2.3. Preparation of $Fe_3O_4/RGO/PAM$ hydrogel

The above mentioned Fe_3O_4/RGO nanocomposites were centrifuged after washing by ethanol, then the precipitate was re-dispersed into 10 mL distilled water. Certain amounts of $Ca(NO_3)_2$ (8 mmol), AM monomer (40 mmol), MBAA (0.013 mmol), and ammonium persulfate (31 mmol) were dissolved in RGO dispersion under N_2 atmosphere in

an ice bath. After degassing for 15 min, the mixture was placed in an oven at 70 °C for 4 h. The 0.1Fe/RGO/PAM, 0.2Fe/RGO/PAM and 0.4Fe/RGO/PAM hydrogels were prepared via adjusting the concentration of $Fe(acac)_3$/ethanol solution to 0.1 mol L^{-1}, 0.2 mol L^{-1}, 0.4 mol L^{-1} during the preparation of Fe_3O_4/RGO process, respectively.

2.4. Characterization

X-ray diffraction (XRD) patterns of all samples were collected in the range 5–80° (2θ) using a RigakuD/MAX 2550 diffract meter (Cu K radiation, =1.5406 Å), operated at 40 kV and 100 mA. The surface morphologies were observed by scanning electron microscopy (JEOL.JSM-6360LV). The elemental analysis was tested by FESEM EDS-mapping (Nova NanoSEM 450). Raman measurements were performed at room temperature using Raman microscopes (Renishaw, UK) under the excitation wavelength of 532 nm. Thermogravimetric and differential thermal analyses were conducted on a Pyris Diamond TG/DTA (PerkinElmer) apparatus at a heating rate of 20 °C min^{-1} from 40 to 800 °C in air flow. Fourier transform infrared spectroscopy (FTIR) spectra were recorded on a Perkin-Elmer Paragon 1000PC spectrometer. The concentration of the pollutant was measured using a UV–vis spectrophotometer (Shimadzu, UV-2450). COD (Hach COD reactor 45600-00/Hach DR 2010 spectrophotometer, colorimetric method 5220 D). The target compounds were identified and quantified by gas chromatograph (GC-2010) interfaced with quadrupole mass spectrometer (QP-2010) (Shimadzu Corporation, Japan).

2.5. Photo-Fenton reaction

All the Photo-Fenton activity tests were performed under Tungsten lamp (> 420 nm, 1000 W). Before the photo-Fenton tests were turned on, the samples, including of RGO/PAM, 0.1Fe/GO/PAM, 0.2Fe/RGO/PAM and 0.4Fe/RGO/PAM hydrogels, should be freeze-dried for 12 h. Thus the obtained aerogels can be tested under visible light. 50 mL RhB
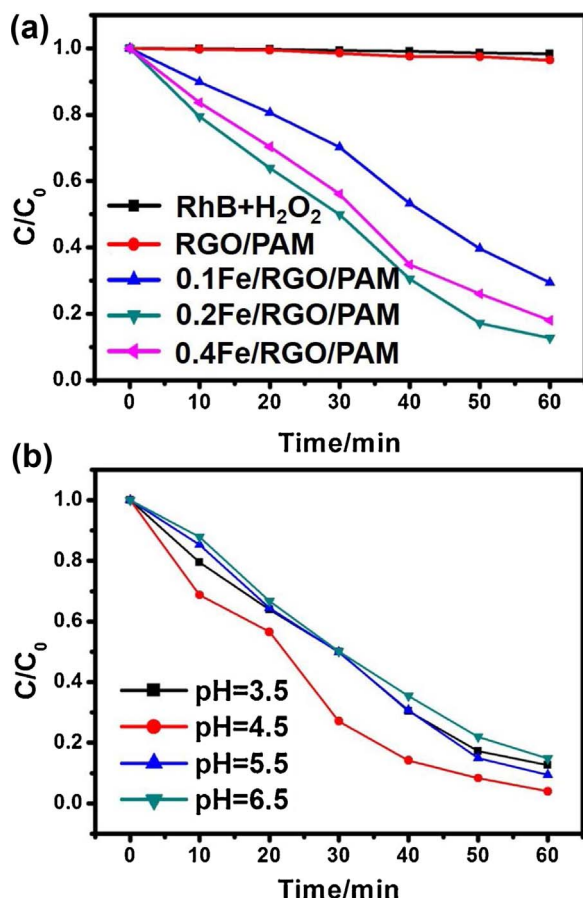
Fig. 6. (a) Photo-Fenton-reaction for the degradation of RhB over different samples (20 mg/L RhB, pH = 3.5, visible light: λ > 420 nm). (b) Photo-Fenton-reaction under different pH values for the degradation of RhB over 0.2Fe/RGO/PAM hydrogel (20 mg/L RhB, visible light: λ > 420 nm).
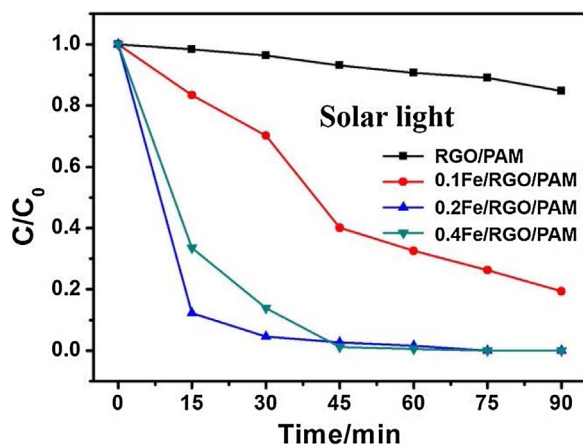

Fig. 7. (a) Photo-Fenton-reaction for the degradation of RhB over different samples (20 mg/L RhB, pH = 4.5, simulated solar light: 300 W Xe with AM 1.5 filter).

solution (20 mg/L) was adjusted at different pH values by adding of H$_2$SO$_4$ solution. Before the hydrogel was irradiated with visible light, 1.0 mL H$_2$O$_2$ were added into the reaction solution. Amount of solution was taken from the reaction cell at given time intervals. The absorbance of RhB solution was measured by an UV–vis spectrometer at 550 nm after full color development.
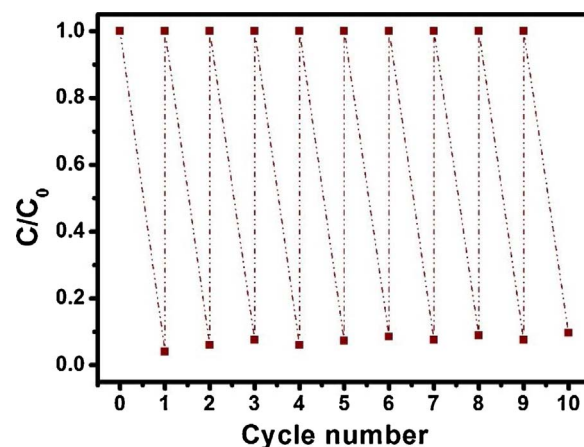

Fig. 8. Cyclic test of 0.2Fe/RGO/PAM for the Photo-Fenton degradation of RhB (20 mg/L RhB, pH = 4.5, visible light irradiation for 1 h every cycle: λ > 420 nm).

2.6. Equilibrium swelling degree of hydrogel

The dried hydrogel was immersed into distilled water until their weight became constant. The hydrogel was then removed from water and weighed. The swelling ratio was calculated as the equation followed by:

$$\text{Swelling ratio} = \frac{Ws - Wd}{Wd}$$

where Wd and Ws represent the weight of the dried hydrogel and the hydrogel at swelling equilibrium state, respectively (Wd = 4.330 g, Ws = 29.4640 g).

Thus, in our work, Swelling ratio = 5.8.

2.7. Solar light assisted cyclic removal of RhB in the flowing system

The flowing degradation system is mainly made of such devices, for instance, condensate tube, beaker, peristaltic pump and mercury lamp (the photograph of device will be shown in Section 3.4). When the pump is working, the RhB solution can flow continuously. Then the Photo-Fenton process was irradiated with simulated solar light (300 W Xe lamp).

2.8. Synchronous removal of organic pollutants and heavy metal ions

Each amount of 150 mg Ce(NO$_3$)$_3$, Cu(NO$_3$)$_2$, AgNO$_3$, Cd(NO$_3$)$_2$ were respectively added into the 50 mL RhB (20 mg/L) solution. After then, 0.2Fe/RGO/PAM hydrogel and 1.0 mL H$_2$O$_2$ were successively put into the above solution. The solution was adjusted the pH value at 4.5 by adding of H$_2$SO$_4$ solution. After one-hour visible light irradiation (halogen tungsten lamp: λ > 420 nm), the absorbance of solution was measured by an UV–vis spectrometer at 550 nm after full color development. After that, the solution was continued to keep in the dark for another two days. After adsorption for two days, the solution was extracted and tested by ICP-EOS to detect the residual heavy metal ions in the solution.

2.9. Degradation of actual industrial sewage

In this part, we aimed to deal with the actual industrial sewage by our prepared hydrogel. The industrial wastewater (benzenoid wastewater) was got from the chemical plant whose original COD is 10400 mg/L. We chose the optimal catalyst of 0.2Fe/RGO/PAM hydrogel for the test. The light source is still Tungsten lamp (> 420 nm, 1000 W). The pH value of swage was adjusted at 3.5 by adding NaOH solution. When the light was turned, 1.0 mL H$_2$O$_2$ was added into the
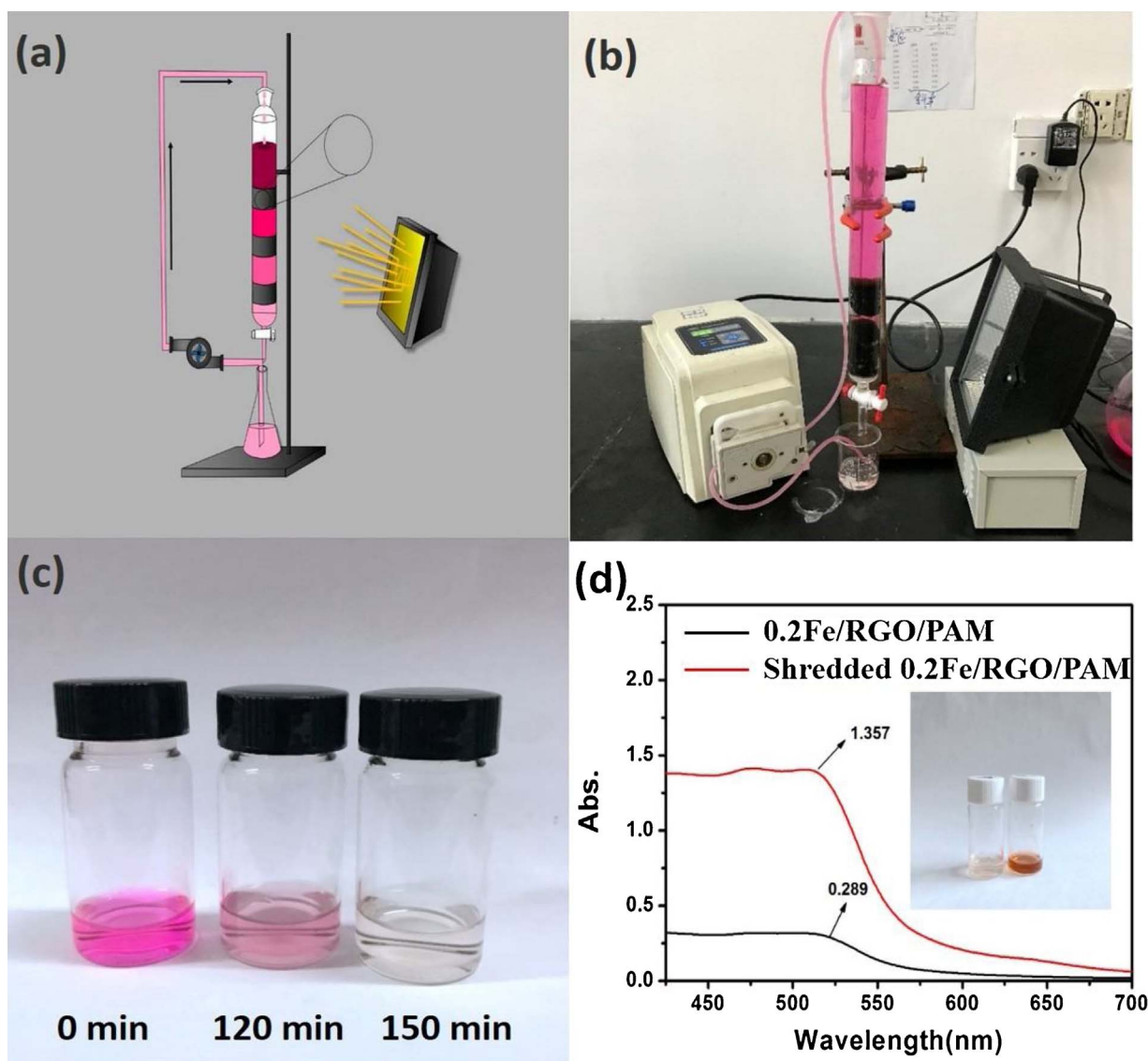
Fig. 9. (a) Conceptual simulation image and (b) actual photograph of our self-designed flowing cyclic degradation system (1.0 mL H_2O_2, 20 mg/L RhB, pH = 4.5, UV light). (c) Extracted RhB solution at different interval time (at 0 min, 120 min, 150 min, respectively). (d) Absorption spectra of RhB filter liquor in the presence of 1, 10-phenanthrolinen monohydrate.
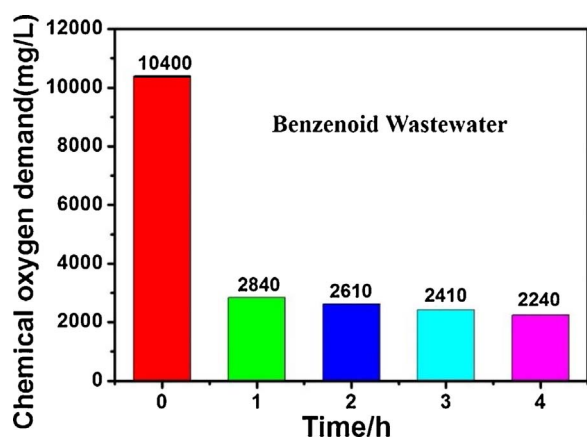

Fig. 10. Photo-Fenton-reaction for the degradation of fine chemical wastewater over 0.2Fe/RGO/PAM (benzenoid wastewater, pH = 4.5, visible light: λ > 420 nm).

actual industrial sewage. Amount of the solution was taken from the reaction cell at given time intervals. After visible-light-Fenton process, the original and reaction solution were all tested by Hach COD reactor

45600-00/Hach DR 2010 spectrophotometer.

3. Results and discussion

3.1. Structure and morphology

The toughly stretchable Fe_3O_4/RGO/PAM hydrogel was synthesized as illustrated in Fig. 1a. The GO sheets were prepared via a modified Hummers' method [34]. And then the Fe_3O_4 nanoparticles were embedded in the RGO sheets by using a Stöber-like method [24]. The Fe_3O_4/RGO was added into a solution including AM monomers, Ca $(NO_3)_2$, MBAA and ammonium persulfate. After the polymerization reaction, a hydrogel of Fe_3O_4/RGO/PAM with a superior stretchability was obtained. To investigate the composition of hydrogel, XRD patterns were obtained over the GO powders, PAM hydrogel, RGO/PAM hydrogel and 0.2Fe/RGO/PAM hydrogel (Fig. 1b). A sharp diffraction peak at the 2θ position of 11.3°, which is indexed to (001) of graphene oxide (GO) [35–37]. The PAM hydrogel presented a broad noncrystal-line diffraction region between 21° and 30°. In terms of RGO/PAM, no obvious diffraction peak existing which is ascribed to the reduction of graphene oxide (RGO). However, for the sample of 0.2Fe/RGO/PAM hydrogel, two diffraction peaks at 22.3° and 28.9° could be observed,
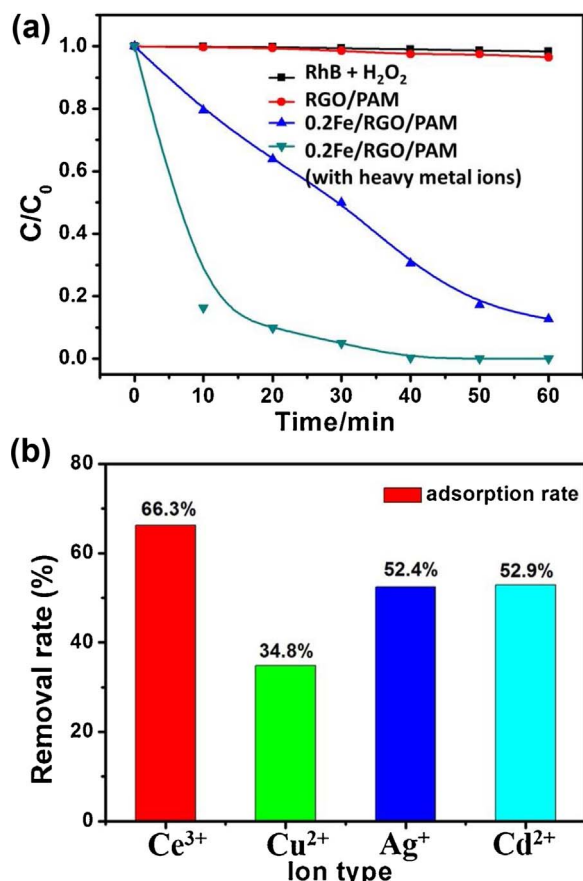
Fig. 11. (a) Photo-Fenton-reaction for the degradation of RhB over hydrogels under different conditions (20 mg/L RhB, pH = 4.5, visible light: λ > 420 nm). (b) Removal rate of heavy metal ions after the degradation of RhB over 0.2Fe/RGO/PAM, hydrogel (adsorption in the dark for two days).

which represent the presence of Fe_3O_4 nanoparticles [24]. Meanwhile, the corresponding Raman characterization of prepared hydrogels are shown in Fig. 1c. After polymerization process, the D- and G-bands shift from 1354.1 cm^{-1} and 1612.3 cm^{-1} to 1351.8 cm^{-1} and 1602.4 cm^{-1}, respectively, indicating the reduction of GO [38]. The increase of the intensity ratio of D/G bands after polymerization process further confirms the reduction of GO [39]. And it also confirms that 0.2Fe/RGO/PAM hydrogel contains a lower percentage of the sp^2 domains, and the PAM was successfully grafted onto the RGO surfaces.

Fig. 2a shows the FT-IR spectra of the GO powders, PAM, RGO/PAM, and 0.2Fe/RGO/PAM hydrogels. The absorption bands before grafting with PAM at 1368.9, 1585.0, 1721.2, and 3370.8 cm^{-1} correspond to C—O bonds, sp^2 C=C bonds, C=O stretching vibrations, and −OH stretching vibrations [40,41], respectively. The peaks around 1665 cm^{-1} among PAM, RGO/PAM and 0.2Fe/RGO/PAM hydrogels are ascribed to the in-plane deformation vibration of N−H. The FT-IR spectrum of the RGO/PAM nanosheets presents a similar characteristic peak related to −OH (3368.3 cm^{-1}) stretching vibrations with that of PAM, which has an obvious decrease after the compounding modification with PAM. It is due to the occurrence of dehydration reaction between GO and PAM. Furthermore, compared with the FTIR spectrum of GO, it is easy to note that there are additional characteristic peaks, such as the double peaks occurring at 1352 cm^{-1} (stretching vibration of −NH groups). These characteristic peaks are in agreement with the infrared spectrum of polyacrylamide, which confirms that PAM has been successfully grafted on RGO. To investigate the thermostability of RGO/PAM and 0.2Fe/RGO/PAM hydrogels, TGA was used to determine the composition and stability, and the results are shown in Fig. 2b. GO is thermally unstable and starts to lose mass below 100 °C, but the

major mass loss occurs at about 200 °C. This is presumably due to pyrolysis of the labile oxygen-containing functional groups to yield CO, CO_2, and steam. The overall weight loss of GO is about 50% at 600 °C, but that for RGO/PAM and 0.2Fe/RGO/PAM (with 10% cross-linking agent) is 90% and 80%, respectively. RGO/PAM and 0.2Fe/RGO/PAM show a similar pattern of weight loss, and both have two major mass losses between 300 °C and 500 °C. That is because of the decomposition and carbonization of PAM [42].

In order to observe the microstructure of Fe_3O_4/RGO/PAM, the hydrogel was cut into pieces for the SEM characterization, as shown in Fig. 3. Compared with the SEM image of RGO/PAM, after introducing Fe_3O_4, the hydrogel displays a rough section (Fig. 3a, b), which implies the high dispersion of Fe_3O_4 nanoparticles into the skeleton of 3D network. The surface of RGO/PAM hydrogel is smooth, and the PAM chains are tightly wrapped by the RGO sheets. Therefore, a uniformly lamellar structure was successfully formed. While Fe_3O_4 nanoparticles were loaded on RGO sheets, in Fig. 3b, the surface of 0.2Fe/RGO/PAM hydrogel obviously exhibits many small protuberances. Fig. 3c exhibits the FESEM-EDS-mapping of the section of 0.2Fe/RGO/PAM hydrogel. The bright regions correspond to the presence of the elements C (green) and Fe (yellow), respectively, indicating the highly dispersed Fe_3O_4 nanoparticles in hydrogel. And the corresponding Fe elemental content from the EDS analysis is 0.24 wt%, implying the Fe_3O_4 particles have been introduced in the hydrogel.

3.2. Mechanical strength property of the hydrogel

The prepared Fe_3O_4/RGO/PAM hydrogel consists of a 3D-RGO network and chemically crosslinked PAM network. The PAM network was fabricated by initiating polymerization of AM monomers in a mixture of $Ca(NO_3)_2$ and Fe_3O_4/RGO sheets dispersion. With the addition of $Ca(NO_3)_2$ into Fe_3O_4/RGO sheets dispersion, the RGO sheets were self-assembly into a 3D network, owing to the coordination of Ca^{2+} with oxygen-containing groups of RGO sheets [43]. When AM monomers dissolving into the above RGO sheets dispersion, MBAA and ammonium persulfate were added to act as the crosslinker and initiator, respectively. Therefore, PAM chains were chemically crosslinked, leading to the formation of the highly stretchable Fe_3O_4/RGO/PAM hydrogel. Interestingly, when the hydrogel is compressed, it will be quickly recovered and the compression stress was released. By analyzing the compress stress (σ)- compress strain (ε) plot, as shown in Fig. 4, the compress strain of 0.2Fe/GO/PAM (0.945) is higher than the pure PAM hydrogel (0.729). Thus, it is revealed that the Fe_3O_4/RGO/ PAM is equipped with high anti-compression property. In addition to the excellent anti-compression property, the hydrogel also has an outstanding tensile property, as shown in Fig. 5. Compared with the hydrogel of PAM without RGO, Fe_3O_4/RGO/PAM hydrogel has a strong mechanical strength, which remained unscathed after a tensile testing.

3.3. Photo-Fenton-reaction for the degradation of organic pollutants

Fenton reaction is well known as one of the most effective Advanced Oxidation Processes (AOPs), due to its high oxidation potential. The generated hydroxyl radicals in Fenton process possess inherent properties that enable it to attack the structure of most of the organic molecules to achieve a complete mineralization of organic pollutants into CO_2, water and mineral acids such as sulfuric, hydrochloric and nitric acids [44–46]. Herein, we replace the conventional Fenton reagent (Fe^{2+}) by our prepared Fe_3O_4/RGO/PAM hydrogels. Additionally, we introduce visible light to test its ability in the degradation of RhB. Before the Fenton reaction, all the hydrogels need to be free-dried to remove all the water. As shown in Fig. 6a, we firstly fix the pH value of the solution at 3.5. By analysis, not only H_2O_2 (1.0 mL) but also RGO/ PAM hydrogel were added into the solution, irradiated by the visible light. Predictably, all the Fe_3O_4/RGO/PAM hydrogels exhibit a higher activity for the degradation of RhB than the RGO/PAM. It is worthy of
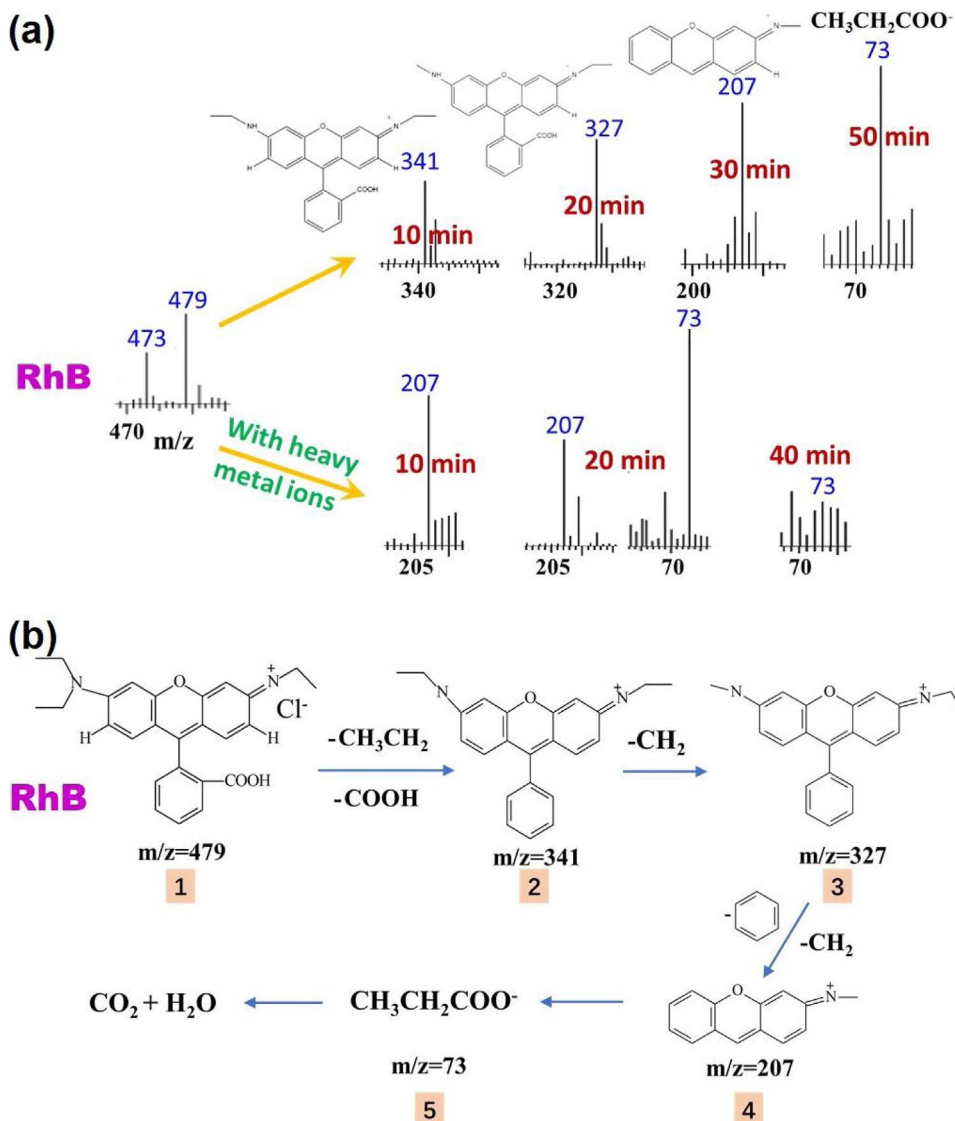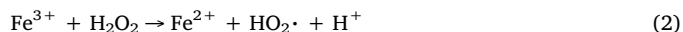
Fig. 12. (a) Mass spectra of intermediates observed in the GC chromatogram that appeared in the degradation process of RhB under different irradiation time. (b) Schematic diagram of Photo-Fenton degradation mechanism of RhB (without heavy metal ions).
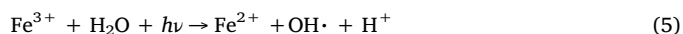
being noted that the catalyst 0.2Fe/RGO/PAM showed the optimal Photo-Fenton activity (up to 90% in 60 min). As we all know, the pH value has a significant role determining the efficiency of Fenton oxidation. Commonly, the pH value is limited in the range of 2.0–4.0[47]. However, in our case, when the pH value continues to increase to 6.5, the degradation rate over 0.2Fe/RGO/PAM is still very high for the degradation of RhB (Fig. 6b). It is interesting to conclude that the pH region can be expanded from 3.5 to 6.5 for the Fenton reaction, which indicates that the hydrogel therefore has a good future of the industrial application.

Furthermore, as shown in Fig. 7, we also investigated the hydrogel's Photo-Fenton efficiency under the simulated solar light (300 W Xe lamp with AM 1.5 filter). Under the solar light irradiation, it was obviously found that the degradation rate for the RhB was further improved, compared with that driven by the visible light (> 420 nm). The degradation rate of the optimal catalyst 0.2Fe/RGO/PAM can achieve 90% within 15 min. The common Fenton reaction mechanism is followed by Eqs. (1)1 and (2). Under the solar light irradiation, the dye molecules like RhB will be sensitized by the photons to release the electrons for the reduction of Fe^{3+}, which is beneficial to the cycle reaction of Fe^{2+}/Fe^{3+} during the Fenton reaction (Eqs. (3) and (4)). It has been found that $Dye^+ \cdot$ could hydrolyze or react with some oxidizer such as the dissolved oxygen molecules in solution [48,49]. Meanwhile, by applying solar light or UV light to the Fenton process, additional

hydroxyl radicals are generated and ferric ions are oxidized into ferrous as shown in Eq. (5). Recycling of Fe^{2+} leads to further generation of OH· according to Eq. (1). The significant increase of the gross of hydroxyl radicals results in the acceleration of the solar-light-driven Fenton reaction for the degradation of organic dyes.

$$Fe^{2+} + H_2O_2 \rightarrow Fe^{3+} + OH\cdot + OH^- \tag{1}$$

$$Fe^{3+} + H_2O_2 \rightarrow Fe^{2+} + HO_2\cdot + H^+ \tag{2}$$

In the presence of solar light:

$$Dye \rightarrow Dye^* \tag{3}$$

$$Dye^* + Fe^{3+} \rightarrow Dye^+\cdot + Fe^{2+} \tag{4}$$

$$Fe^{3+} + H_2O + h\nu \rightarrow Fe^{2+} + OH\cdot + H^+ \tag{5}$$

3.4. Reversibility and flowing cyclic degradation system

In order to exam the stability and reversibility of the Fe_3O_4/RGO/PAM hydrogels in the Photo-Fenton-reaction, we have done the cyclic test for the degradation of RhB under the visible light irradiation, as shown in Fig. 8. After 10 cycles, the removal efficiency of RhB is still very high and remained at 90%. Thus, we can conclude that such highly

elastic and super stretchable Fe_3O_4/RGO/PAM hydrogel not only possesses highly efficient Photo-Fenton activity but also has excellent reversibility.

According to above mentioned experimental details and specific analysis, we have proposed a novel idea that whether the hydrogel can be used in a flowing degradation system or not for the degradation of organic pollutants. Thus, we specifically set up the device, as shown in Fig. 9a, b, which is composed of condensate tube, beaker, peristaltic pump and mercury lamp. Herein, the UV light was employed for the Fenton reaction. The extracted solutions at different time (0 min, 120 min, 150 min) were placed from the left to right in Fig. 9c. When time arrives at 120 min, the solution starts to exhibit a little pink color. At 150 min, the solution in the device shows colorless. To emphasize the advantage of 3D structure for restraining the dissolution of ferric ions, we make a comparison on the dissolution of ferrous ions between the bulk hydrogel and the ground one (Fig. 9d). We used the 1,10-phenanthrolinen monohydrate as the chromogenic agent for the detection of Fe^{2+} ions in the solution [24]. After sufficient grinding, the hydrogel fell to pieces. Seen from the UV–vis absorption spectra of the solution, the intensity of absorption peak at 523 nm increases from 0.289 to 1.357 after the grinding treatment. It indicates that the ferrous ions can be well confined in the bulk of hydrogel before grinding, which could greatly prevent the generation of iron cements like $Fe(OH)_3$ and promote the stability of Fenton reaction [22].

3.5. Fine chemical wastewater treatment

Fine chemical wastewater is a typical industrial organic and non-biodegradable wastewater with high strength of COD, ammonia nitrogen and deep color. As known to all, the discharge of fine chemical wastewater has dramatically increased, ascribing to the rapid development of economy. In order to highlight the advantage of Fe_3O_4/RGO/PAM hydrogel for the degradation of industrial sewage, we carried out the Photo-Fenton reaction for the degradation of fine chemical wastewater (benzenoid wastewater), which is the original water of the chemical factory and its COD reaches to 10400 mg/L. As can be seen in Fig. 10, after irradiation with visible light for 1 h, the COD of sewage has dropped from 10400 to 2840 mg/L. Then, the COD value is stable in the range of 2200–2800 mg/L in the following several hours. According to the trend, the organic pollutants in sewage have been removed about 73% during the first hour. Thus, it can be inferred that our prepared Fe_3O_4/RGO/PAM hydrogel can be directly used in dealing with the industrial sewage.

3.6. Synchronous removal of organic pollutants and heavy metal ions

On one hand, due to the excessive industrialization and urbanization, the content of heavy metal ions in water has escalated rapidly. On the other hand, an effective removal of heavy metal ions from industrial effluents or water is crucial to the society and humans, owing to their toxic nature and other adverse effects on many life entities. Various treatment methods, for instance, ion exchange, reverse osmosis, adsorption, and precipitation have been extensively investigated to remove metal ions from waste [50,51]. Among these methods, adsorption is widely accepted. Amounts of studies concerning on the using of hydrogels with functional groups as the adsorbent for the removal of heavy metal ions have been reported [14]. However, there is less report on using the hydrogel as the catalyst and the adsorbent for the synchronous removal of organic pollutants and heavy metal ions. In this work, we aim to employ the Fe_3O_4/RGO/PAM hydrogel as the adsorbent and Fenton reagent for the removal of heavy metal ions and RhB at one time. We take the optimal catalyst of 0.2Fe/RGO/PAM for example, a hydrogel was added into a 50 mL simulated wastewater, which includes $Ce(NO_3)_3$, $Cu(NO_3)_2$, $AgNO_3$, $Cd(NO_3)_2$ and RhB (20 mg/L). Interestingly, the degradation rate of RhB can be up to 90% within 20 min visible light irradiation, which is much higher than that

of the hydrogel in the absence of heavy metal ions (Fig. 11a). That is because the heavy metal ions like Ce^{3+} [52,53] and Cu^{2+} [54,55] also can decompose the H_2O_2 to release hydroxyl radicals like the Fe^{2+}. The elements copper and cerium have the similar Fenton-like mechanism.

After the degradation of RhB, the wastewater solution continued to react in the dark for another two days. After that, we took the original and extracted solution to be characterized by ICP-EOS for the detection of residua heavy metal ions. Seen Fig. 11b, different metal ions adsorption capacity over 0.2Fe/RGO/PAM hydrogel has sorted as follows: Ce^{3+}(66.3%) > Cd^{2+}(52.9%) > Ag^+(52.4%) > Cu^{2+}(34.8%). And the adsorption is mainly caused by chemical interaction. On one hand, the he higher the valence of metal ions, the affinity ascribed to the coordination (formation of inner sphere complexes) with the carboxylic acid groups will be much stronger [56]. On the other hand, the amide groups may play a secondary role in combination with metal ions [57]. All these data show that Fe_2O_3/RGO/PAM hydrogels possess great potential for the synchronous removal of organic pollutants and heavy metal ions from industrial wastewater.

To further investigate the Photo-Fentoin-reaction mechanism for the degradation of RhB, we employed the gas chromatography-mass spectrometry (GC–MS) to analyze the degradation progress of RhB molecular, as shown in Fig. 12. The GC–MS spectra of original RhB is shown in Fig. 12a. The mass peaks at m/z 479 and 473 are those of RhB and its N-deethylated intermediates [58]. When there is absence of heavy metal ions in the solution for the degradation of RhB, with the growing of light irradiation, it is successive appearing the new peaks at m/z 341, 327, 207 and 73, which are assigned to $C_{23}H_{22}ON_2^+$, $C_{22}H_{20}ON_2$, $C_{14}H_{11}ON$ and $CH_3CH_2COO^-$, respectively (Fig. 12a). The scheme of degradation for RhB is shown in Fig. 12b. When Photo-Fenton-reaction happening at 10 min, the parent ion ($m/z = 341$) is shown in Fig. 12b, whose structure corresponds to Structure 2. This step accompanies with the deethylation and decarboxylation. At 20 min, the Fenton process keeps demethylating (Structure 3). At 30 min, this step continues to decompose molecule of Structure 3 into Structure 4. When irradiation for 50 min, the whole solution is mainly composed of Structure 5. That means, the RhB is fundamentally decomposed into propionic acid. Interestingly, if the heavy metal ions (Ce^{3+}, Cu^{2+}, Ag^+, Cd^{2+}) were existing at once in the RhB solution, the RhB molecular can be quickly cracked into Structure 4 within 10 min irradiation. Then, after irradiation for 20 min, the solution is mainly composed of Structure 4 and 5. The peak at m/z 73 has a distinct decrease when the irradiation time prolonged to 40 min, which implies that most of RhB molecular has been decomposed into CO_2 and H_2O.

4. Conlusions

In summary, to deal with the industrial wastewater contained heavy metal ions and organic pollutants, the Fe_3O_4/RGO/PAM hydrogel has some special advantages. That is the hydrogel can adsorb the heavy metal ions owing to its 3D-network structure, meanwhile, the presence of metal ions also can greatly accelerate the Photo-Fenton-reaction over the hydrogel for the degradation of organic pollutants. Hence, our research provides a new way to process the organic wastewater of high consistence and difficult decomposition.

Author contributions

The manuscript was written through contributions of all authors. All authors have given approval to the final version of the manuscript.

Notes

The authors declare no competing financial interest.

Acknowledgments

References

[1] R.G. Zepp, B.C. Faust, J. Hoigne, Hydroxyl radical formation in aqueous reactions (pH 3–8) of iron(II) with hydrogen peroxide: the photo-Fenton reaction, Environ. Sci. Technol. 26 (1992) 313–319.

[2] Y. Zhang, N. Klamerth, P. Chelme-Ayala, M. Gamal El-Din, Comparison of nitrilotriacetic acid and [S,S]-ethylenediamine-N,N'-disuccinic acid in UV-Fenton for the treatment of oil sands process-affected water at natural pH, Environ, Sci. Technol. 50 (2016) 10535–10544.

[3] R. Martín, S. Navalon, M. Alvaro, H. Garcia, Optimized water treatment by combining catalytic Fenton reaction using diamond supported gold and biological degradation, Appl. Catal. B Environ. 103 (2011) 246–252.

[4] I. Catanzaro, G. Avellone, G. Marc, M. Saverini, L. Scalici, G. Sciandrello, L. Palmisano, Biological effects and photodegradation by TiO$_2$ of terpenes present in industrial wastewater, J. Hazard. Mater. 185 (2011) 591–597.

[5] B.A. Getachew, S.-R. Kim, J.-H. Kim, Self-Healing hydrogel pore-filled water filtration membranes, Environ. Sci. Technol. 51 (2017) 905–913.

[6] G.A. Borges, L.P. Silva, J.A. Penido, L.R. de Lemos, A.B. Mageste, G.D. Rodrigues, A method for dye extraction using an aqueous two-phase system: effect of co-occurrence of contaminants in textile industry wastewater, J. Environ. Manag. 183 (Part 1) (2016) 196–203.

[7] A. Abou-Shady, Recycling of polluted wastewater for agriculture purpose using electrodialysis: perspective for large scale application, Chem. Eng. J. 323 (2017) 1–18.

[8] G. Chen, A.S. Hoffman, Graft copolymers that exhibit temperature-induced phase transitions over a wide range of pH, Nature 373 (1995) 49–52.

[9] Z. Ge, J. Hu, F. Huang, S. Liu, Responsive supramolecular gels constructed by crown ether based molecular recognition, Angew. Chem. 121 (2009) 1830–1834.

[10] F. Ilmain, T. Tanaka, E. Kokufuta, Volume transition in a gel driven by hydrogen bonding, Nature 349 (1991) 400–401.

[11] D.J. Pochan, J.P. Schneider, J. Kretsinger, B. Ozbas, K. Rajagopal, L. Haines, Thermally reversible hydrogels via intramolecular folding and consequent self-assembly of a de novo designed peptide, J. Am. Chem. Soc. 125 (2003) 11802–11803.

[12] N. Bhattarai, J. Gunn, M. Zhang, Chitosan-based hydrogels for controlled, localized drug delivery, Adv. Drug Deliv. Rev. 62 (2010) 83–99.

[13] D. Seliktar, Designing cell-compatible hydrogels for biomedical applications, Science 336 (2012) 1124.

[14] M. Zhang, L. Song, H. Jiang, S. Li, Y. Shao, J. Yang, J. Li, Biomass based hydrogel as an adsorbent for the fast removal of heavy metal ions from aqueous solutions, J. Mater. Chem. A 5 (2017) 3434–3446.

[15] M. Khan, I.M.C. Lo, A holistic review of hydrogel applications in the adsorptive removal of aqueous pollutants: recent progress, challenges, and perspectives, Water Res. 106 (2016) 259–271.

[16] D. Su, M. Yao, J. Liu, Y. Zhong, X. Chen, Z. Shao, Enhancing mechanical properties of silk fibroin hydrogel through restricting the growth of β-sheet domains, ACS Appl. Mater. Interface 9 (2017) 17489–17498.

[17] Y. Okumura, K. Ito, The polyrotaxane gel: a topological gel by figure-of-eight cross-links, Adv. Mater. 13 (2001) 485–487.

[18] J.P. Gong, Why are double network hydrogels so tough? Soft Matter 6 (2010) 2583–2590.

[19] K. Haraguchi, T. Takehisa, Nanocomposite hydrogels: a unique organic-inorganic network structure with extraordinary mechanical, optical, and swelling/de-swelling properties, Adv. Mater. 14 (2002) 1120.

[20] W.L. Hom, S.R. Bhatia, Significant enhancement of elasticity in alginate-clay nanocomposite hydrogels with PEO-PPO-PEO copolymers, Polymer 109 (2017) 170–175.

[21] M. Xing, F. Shen, B. Qiu, J. Zhang, Highly-dispersed boron-doped graphene nanosheets loaded with TiO$_2$ nanoparticles for enhancing CO$_2$ photoreduction, Sci. Rep. 4 (2014).

[22] B. Qiu, M. Xing, J. Zhang, Stöber-like method to synthesize ultralight porous, stretchable Fe$_2$O$_3$/graphene aerogels for excellent performance in photo-Fenton reaction and electrochemical capacitors, J. Mater. Chem. A 3 (2015) 12820–12827.

[23] B. Qiu, M. Xing, J. Zhang, Mesoporous TiO$_2$ nanocrystals grown in situ on graphene aerogels for high photocatalysis and lithium-ion batteries, J. Am. Chem. Soc. 136 (2014) 5852–5855.

[24] B. Qiu, Q. Li, B. Shen, M. Xing, J. Zhang, Stöber-like method to synthesize ultra-dispersed Fe$_3$O$_4$ nanoparticles on graphene with excellent Photo-Fenton reaction and high-performance lithium storage, Appl. Catal. B Environ. 183 (2016) 216–223.

[25] J. Shen, B. Yan, T. Li, Y. Long, N. Li, M. Ye, Mechanical, thermal and swelling properties of poly(acrylic acid)-graphene oxide composite hydrogels, Soft. Matter 8 (2012) 1831–1836.

[26] R. Liu, S. Liang, X.-Z. Tang, D. Yan, X. Li, Z.-Z. Yu, Tough and highly stretchable graphene oxide/polyacrylamide nanocomposite hydrogels, J. Mater. Chem. 22 (2012) 14160–14167.

[27] H.P. Cong, P. Wang, S.H. Yu, Highly elastic and superstretchable graphene oxide/polyacrylamide hydrogels, Small 10 (2014) 448–453.

[28] G.K. Ramesha, A. Vijaya Kumara, H.B. Muralidhara, S. Sampath, Graphene and graphene oxide as effective adsorbents toward anionic and cationic dyes, J. Colloid Interface Sci. 361 (2011) 270–277.

[29] J. Fan, Z. Shi, M. Lian, H. Li, J. Yin, Mechanically strong graphene oxide/sodium alginate/polyacrylamide nanocomposite hydrogel with improved dye adsorption capacity, J. Mater. Chem. A 1 (2013) 7433–7443.

[30] F. Fu, Q. Wang, Removal of heavy metal ions from wastewaters: a review, J. Environ. Manag. 92 (2011) 407–418.

[31] Y. Zhao, Y. Chen, M. Li, S. Zhou, A. Xue, W. Xing, Adsorption of Hg^{2+} from aqueous solution onto polyacrylamide/attapulgite, J. Hazard. Mater. 171 (2009) 640–646.

[32] N. Todorova, T. Giannakopoulou, N. Boukos, E. Vermisoglou, C. Lekakou, C. Trapalis, Self-propagating solar light reduction of graphite oxide in water, Appl. Surf. Sci. 391 (2017) 601–608.

[33] D. Xu, B. Cheng, S. Cao, J. Yu, Enhanced photocatalytic activity and stability of Z-scheme Ag$_2$CrO$_4$-GO composite photocatalysts for organic pollutant degradation, Appl. Catal. B Environ. 164 (2015) 380–388.

[34] W.S. Hummers Jr., R.E. Offeman, Preparation of graphitic oxide, J. Am. Chem. Soc. 80 (1958) 1339–1339.

[35] C. Lai, M.-M. Wang, G.-M. Zeng, Y.-G. Liu, D.-L. Huang, C. Zhang, R.-Z. Wang, P. Xu, M. Cheng, C. Huang, H.-P. Wu, L. Qin, Synthesis of surface molecular imprinted TiO$_2$/graphene photocatalyst and its highly efficient photocatalytic degradation of target pollutant under visible light irradiation, Appl. Surf. Sci. 390 (2016) 368–376.

[36] S.O.B. Oppong, W.W. Anku, S.K. Shukla, P.P. Govender, Synthesis and characterisation of neodymium doped-zinc oxide–graphene oxide nanocomposite as a highly efficient photocatalyst for enhanced degradation of indigo carmine in water under simulated solar light, Res. Chem. Intermed. 43 (2017) 481–501.

[37] M. Moshari, M. Rabbani, R. Rahimi, Synthesis of TCPP–Fe$_3$O$_4$@S/RGO and its application for purification of water, Res. Chem. Intermed. 42 (2016) 5441–5455.

[38] Q. Xiang, J. Yu, M. Jaroniec, Enhanced photocatalytic H$_2$-production activity of graphene-modified titania nanosheets, Nanoscale 3 (2011) 3670–3678.

[39] L. Xiao, D. Wu, S. Han, Y. Huang, S. Li, M. He, F. Zhang, X. Feng, Self-assembled Fe$_2$O$_3$/graphene aerogel with high lithium storage performance, ACS Appl. Mater. Interface 5 (2013) 3764–3769.

[40] Y. Sun, Q. Wang, C. Chen, X. Tan, X. Wang, Interaction between Eu (III) and graphene oxide nanosheets investigated by batch and extended X-ray absorption fine structure spectroscopy and by modeling techniques, Environ. Sci. Technol. 46 (2012) 6020–6027.

[41] N.A. Kumar, H.-J. Choi, Y.R. Shin, D.W. Chang, L. Dai, J.-B. Baek, Polyaniline-grafted reduced graphene oxide for efficient electrochemical supercapacitors, ACS Nano 6 (2012) 1715–1723.

[42] N. Zhang, R. Li, L. Zhang, H. Chen, W. Wang, Y. Liu, T. Wu, X. Wang, W. Wang, Y. Li, Actuator materials based on graphene oxide/polyacrylamide composite hydrogels prepared by in situ polymerization, Soft. Matter 7 (2011) 7231–7239.

[43] S. Park, K.-S. Lee, G. Bozoklu, W. Cai, S.T. Nguyen, R.S. Ruoff, Graphene oxide papers modified by divalent ions-enhancing mechanical properties via chemical cross-linking, ACS Nano 2 (2008) 572–578.

[44] S. Contreras, M. Rodríguez, E. Chamarro, S. Esplugas, UV-and UV/Fe (III)-enhanced ozonation of nitrobenzene in aqueous solution, J. Photochem. Photobiol. A Chem. 142 (2001) 79–83.

[45] J.M. Joseph, R. Varghese, C. Aravindakumar, Photoproduction of hydroxyl radicals from Fe (III)-hydroxy complex: a quantitative assessment, J. Photochem. Photobiol. A Chem. 146 (2001) 67–73.

[46] M. Rodríguez, N.B. Abderrazik, S. Contreras, E. Chamarro, J. Gimenez, S. Esplugas, Iron (III) photoxidation of organic compounds in aqueous solutions, Appl. Catal. B Environ. 37 (2002) 131–137.

[47] L. Clarizia, D. Russo, I. Di Somma, R. Marotta, R. Andreozzi, Homogeneous photo-Fenton processes at near neutral pH: A review, Appl. Catal. B Environ. 209 (2017) 358–371.

[48] S. Rahhal, H.W. Richter, Reduction of hydrogen peroxide by the ferrous iron chelate of diethylenetriamine-N, N N', N, N-pentaacetate, J. Am. Chem. Soc. 110 (1988) 3126–3133.

[49] N. Colclough, J.R.L. Smith, A mechanistic study of the oxidation of phenols in aqueous solution by oxoiron (IV) tetra (N-methylpyridyl) porphyrins. A model for horseradish peroxidase compound II? J. Chem. Soc. Perk. Trans. 2 (1994) 1139–1149.

[50] W.W. Ngah, C. Endud, R. Mayanar, Removal of copper (II) ions from aqueous solution onto chitosan and cross-linked chitosan beads, React. Funct. Polym. 50 (2002) 181–190.

[51] R. Saliba, H. Gauthier, R. Gauthier, M. Petit-Ramel, Adsorption of copper (II) and chromium (III) ions onto amidoximated cellulose, J. Appl. Polym. Sci. 75 (2000) 1624–1631.

[52] E.G. Heckert, S. Seal, W.T. Self, Fenton-like reaction catalyzed by the rare earth inner transition metal cerium, Environ. Sci. Technol. 42 (2008) 5014–5019.

[53] L. Xu, J. Wang, Magnetic Nanoscaled Fe$_3$O$_4$/CeO$_2$ composite as an efficient Fenton-like heterogeneous catalyst for degradation of 4-chlorophenol, Environ. Sci. Technol. 46 (2012) 10145–10153.

[54] D.A. Nichela, A.M. Berkovic, M.R. Costante, M.P. Juliarena, F.S.G. Einschlag, Nitrobenzene degradation in Fenton-like systems using cu (II) as catalyst.

comparison between Cu (II)-and Fe (III)-based systems, Chem. Eng. J. 228 (2013) 1148–1157.

[55] A.M. Fleming, J.G. Muller, I. Ji, C.J. Burrows, Characterization of 2'-deox-yguanosine oxidation products observed in the Fenton-like system Cu (II)/H_2O_2/ reductant in nucleoside and oligodeoxynucleotide contexts, Org. Biomol. Chem. 9 (2011) 3338–3348.

[56] W. Li, H. Zhao, P.R. Teasdale, R. John, S. Zhang, Synthesis and characterisation of a polyacrylamide–polyacrylic acid copolymer hydrogel for environmental analysis of Cu and Cd, React. Funct. Polym. 52 (2002) 31–41.

[57] P. Liu, J. Guo, Polyacrylamide grafted attapulgite (PAM-ATP) via surface-initiated atom transfer radical polymerization (SI-ATRP) for removal of Hg(II) ion and dyes, Colloid Surf. A Physicochem. Eng. Aspects 282 (2006) 498–503.

[58] K. Yu, S. Yang, H. He, C. Sun, C. Gu, Y. Ju, Visible light-driven photocatalytic de-gradation of Rhodamine B over $NaBiO_3$: pathways and mechanism, J. Phys. Chem. A 113 (2009) 10024–10032.